

STELLAR TIDAL DISRUPTION EVENTS BY DIRECT COLLAPSE BLACK HOLES

KAZUMI KASHIYAMA¹ AND KOHEI INAYOSHI²¹Einstein Fellow–Theoretical Astrophysics Center, Department of Astronomy, University of California, Berkeley, CA 94720, USA and²Simons Society of Fellows–Department of Astronomy, Columbia University, 550 West 120th Street, New York, NY 10027, USA

ABSTRACT

We analyze the early growth stage of direct-collapse black holes (DCBHs) with $\sim 10^5 M_\odot$, which are formed by collapse of supermassive stars in atomic-cooling halos at $z \gtrsim 10$. A nuclear accretion disk around a newborn DCBH is gravitationally unstable and fragments into clumps with a few $10 M_\odot$ at $\sim 0.01 - 0.1$ pc from the center. Such clumps evolve into massive population III stars with a few $10 - 100 M_\odot$ via successive gas accretion and a nuclear star cluster is formed. Radiative and mechanical feedback from an inner slim disk and the star cluster will significantly reduce the gas accretion rate onto the DCBH within $\sim 10^6$ yr. Some of the nuclear stars can be scattered onto the loss cone orbits also within $\lesssim 10^6$ yr and tidally disrupted by the central DCBH. The jet luminosity powered by such tidal disruption events can be $L_j \gtrsim 10^{50}$ erg s⁻¹. The prompt emission will be observed in X-ray bands with a peak duration of $\delta t_{\text{obs}} \sim 10^{5-6} (1+z)$ s followed by a tail $\propto t_{\text{obs}}^{-5/3}$, which can be detectable by *Swift* BAT and eROSITA even from $z \sim 20$. Follow-up observations of the radio afterglows with, e.g., eVLA and the host halos with JWST could probe the earliest AGN feedback from DCBHs.

Subject headings: black hole physics – galaxies: high-redshift – stars: population III – X-rays: bursts

1. INTRODUCTION

In the last decades, high- z quasar surveys have discovered supermassive black holes (SMBHs) with $M_\bullet \gtrsim 10^9 M_\odot$ at $z > 6$ (e.g. Mortlock et al. 2011; Wu et al. 2015), which pose questions about the earliest coevolution of SMBHs and their host galaxies. The observations indicate that at least a minor fraction of high- z BHs experience an extremely efficient mass gain. Several scenarios have been proposed (e.g., Volonteri 2012; Haiman 2013, and references therein). In order to discriminate them, it is important to clarify observational signatures of rapidly growing high- z BHs in the light of the capability of ongoing and upcoming facilities.

Here, we focus on high- z SMBH formation through collapse of supermassive stars (SMSs) with $\gtrsim 10^5 M_\odot$. SMSs can be formed from pristine gas in the so called atomic-cooling halo where radiative cooling by atomic hydrogen (H) is relevant instead by molecular-hydrogen (H₂) (Bromm & Loeb 2003; Begelman et al. 2006; Lodato & Natarajan 2006). Formation of H₂ can be suppressed by Lyman-Werner and H⁻ photodissociation photons from nearby star-forming galaxies (Omukai 2001; Shang et al. 2010; Visbal et al. 2014; Sugimura et al. 2014; Agarwal et al. 2015), and/or collisional dissociation triggered by galactic shocks (Inayoshi & Omukai 2012; Inayoshi et al. 2015). Once $\gtrsim 10^5 M_\odot$ of such a gas is assembled, it becomes Jeans unstable and collapses to form a supermassive protostar at the center (Inayoshi et al. 2014; Becerra et al. 2015; Latif et al. 2016). After \sim Myr of gas accretion, the SMS becomes as massive as $\sim 10^5 M_\odot$ (Hosokawa et al. 2012, 2013; Inayoshi et al. 2013) and can directly collapse into a SMBH due to the general-relativistic instability (Iben

1963; Chandrasekhar 1964; Baumgarte & Shapiro 1999; Shibata & Shapiro 2002; Reisswig et al. 2013). Such direct-collapse black holes (DCBHs) are an attractive candidate of seeds of observed high- z SMBHs.

In the very early growth stage of a DCBH, gas accretion onto the nascent DCBH will result in feedback on the surrounding medium, which might be probed by James Webb Space Telescope (JWST; Gardner et al. 2006) or future 30-40 meter class telescopes, as argued in e.g., Johnson et al. (2011). However, given the field of view (2.2×4.4 arcmin² for JWST NIRC2), a blind search is not necessarily an efficient way to identify newborn DCBHs and their host halos because DCBH formation may be rare in the early Universe. Also we note that X-ray emission from steady accretion onto DCBHs may be challenging to detect even with Chandra (e.g., Hartwig et al. 2015). An alternative strategy is to first find candidates by some transient signatures with survey facilities e.g., *Swift* BAT (Gehrels et al. 2004) and then to do followup observations with e.g., JWST. For example, Matsumoto et al. (2015a,b) argued that ultra-long gamma-ray bursts may accompany DCBH formation.

Here, we propose that tidal disruption events (TDEs) of stars formed in the nuclear accretion disk by a newborn DCBHs could occur. As we discuss later, associated X-ray bursts and radio afterglows may be much brighter than TDEs in the Universe today and could be detected by all-sky instruments such as BAT and eROSITA (Merloni et al. 2012) and on-going radio facilities like the Expanded Very Large Array (eVLA) even from $z \sim 20$.

This paper is organized as follows. In Sec. 2, we analyze a nuclear accretion disk around a newborn DCBH. First we study disk fragmentation and massive population III (Pop III) star formation in the outer disk, and then discuss properties of the inner slim disk. In Sec. 3, we show that TDEs of the massive Pop III stars by the central DCBH are feasible in the early growth stage and consider the observational signatures. We summarize our

¹ kashiyama@berkeley.edu² inayoshi@astro.columbia.edu

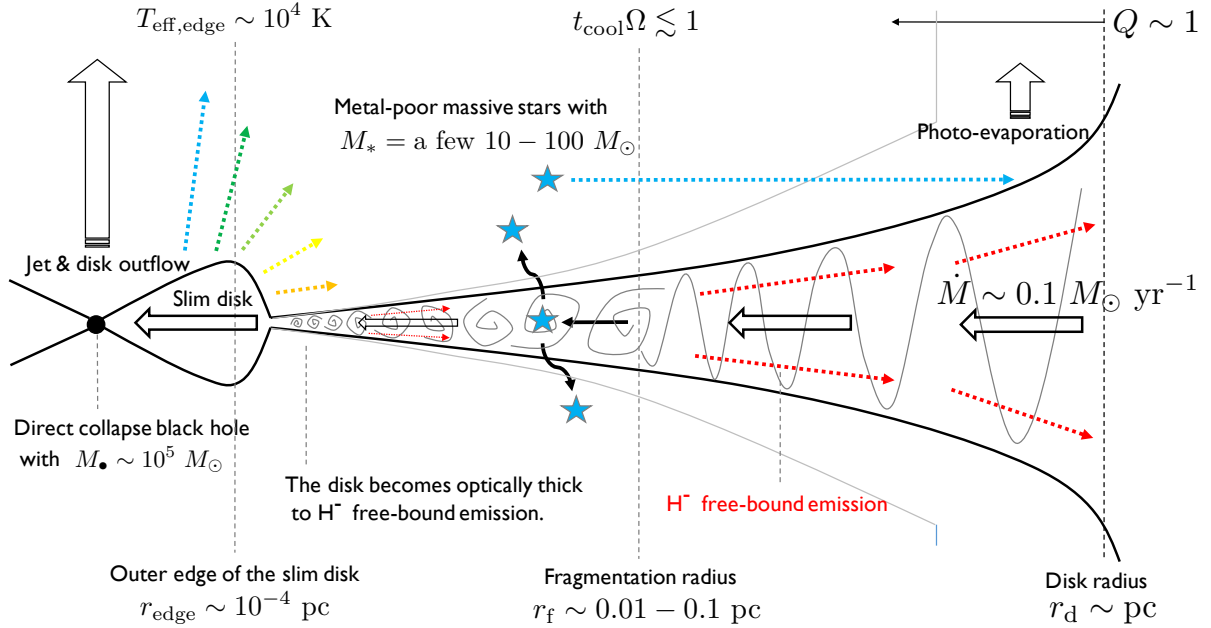


FIG. 1.— Schematic picture of a nuclear accretion disk of a direct collapse black hole within a few Myr after its formation.

paper in Sec. 4.

2. NUCLEAR ACCRETION DISK AROUND DIRECT COLLAPSE BLACK HOLES

We consider a H_2 -free gas cloud with $\gtrsim 10^5 M_\odot$ collapsing isothermally by H cooling ($\text{Ly}\alpha$, two-photon, H^- free-bound, free-free emission) in an atomic-cooling halo with typically $\sim 10^{7-8} M_\odot$. First, a proto-SMS with $\sim 1 - 10 M_\odot$ and a radius of $\sim 10^3 R_\odot$ is formed at the core (Inayoshi et al. 2014; Becerra et al. 2015; Latif et al. 2016). The gas accretion rate onto the core is very high;

$$\dot{M} \approx \frac{c_s^3}{G} \sim 0.095 M_\odot \text{ yr}^{-1} \left(\frac{T_{\text{vir}}}{8000 \text{ K}} \right)^{3/2}, \quad (1)$$

where $c_s = (k_B T / \mu m_p)^{1/2}$ is the sound velocity. As for the mean molecular weight, we set $\mu = 1.22$ assuming the pristine abundance (see Sec. 2.4 for the effect of metal and dust). Note that the above accretion rate is conservative and can be larger than $\sim 1 M_\odot \text{ yr}^{-1}$ for massive atomic-cooling halos (Wise et al. 2008; Regan & Haehnelt 2009a,b). The proto-SMS grows via accretion through a massive self-gravitating disk with a size of $r_d \sim 1 \text{ pc}$ (e.g., Regan et al. 2014), to become a SMS with $\sim 10^5 M_\odot$ (e.g., Hosokawa et al. 2012, 2013; Inayoshi et al. 2013; Schleicher et al. 2013; Inayoshi & Haiman 2014), and then, to collapse into a DCBH (e.g., Shibata & Shapiro 2002; Reisswig et al. 2013). The total gas mass in the atomic cooling halo is sufficient to supply gas onto the nuclear disk at a rate as high as Eq. (1) even after the DCBH is formed unless radiative feedback has been turned on (see Sec. 2.3).

2.1. Outer thin disk

The outer part of the nuclear accretion disk will be self-gravitating and the gas angular momentum can be

transferred mainly by turbulent viscosity due to gravitational instability. The turbulence also heats the disk and can keep the disk marginally stable, i.e., the Toomre parameter

$$Q \equiv \frac{c_s \Omega}{\pi G \Sigma} \sim 1, \quad (2)$$

as long as the cooling time of the disk is sufficiently longer than the dynamical time. Here, Ω is the orbital frequency of the disk and Σ is the disk surface mass density, which is given by

$$\Sigma = \frac{\dot{M}}{3\pi\nu}. \quad (3)$$

We parameterize the disk viscosity as

$$\nu = \alpha c_s h \quad (4)$$

(Shakura & Sunyaev 1973), where

$$h = c_s / \Omega \quad (5)$$

is the disk scale height. The equation of the heat balance is given by

$$\frac{9}{4} \nu \Sigma \Omega^2 = 2h \Lambda_{\text{H}^-}, \quad (6)$$

where the left and right hand side represents the viscous heating and radiative cooling, respectively. As for the radiative cooling rate (in units of $\text{erg s}^{-1} \text{ cm}^{-3}$), we use an approximate formula (Inayoshi & Haiman 2014)¹;

$$\Lambda_{\text{H}^-} \approx 5.0 \times 10^{-41} T^{2.2} n^{5/2} e^{-\frac{1.27 \times 10^5}{2T}}, \quad (7)$$

where T is the disk temperature in unit of Kelvin and

$$n = \frac{\Sigma}{\mu m_p (2h)}. \quad (8)$$

¹ We set the mean molecular weight of the gas to $\mu = 1.22$. This makes the disk fragmentation radius a factor smaller than that obtained by Inayoshi & Haiman (2014) with $\mu = 2.0$.

is the number density of hydrogen nuclei in unit of cm^{-3} . Eq. (7) is valid for dense ($n \gtrsim 10^8 \text{ cm}^{-3}$) and warm ($3000 \text{ K} \lesssim T \lesssim 8000 \text{ K}$) pristine gas, which is predominantly neutral and optically thin, and the main cooling process is free-bound emission of H^- ions ($\text{H} + \text{e}^- \rightarrow \text{H}^- + \gamma$, Omukai 2001). From Eqs. (2-8), we can obtain the radial profile of the outer disk, Σ , h , T and α for a fixed (\dot{M}, Q) as a function of Ω or distance from the center, $r = (GM_\bullet/\Omega^2)^{1/3}$, where M_\bullet is the mass of the DCBH.

2.1.1. Disk fragmentation

Once the cooling time and dynamical time becomes comparable, the disk will fragment into clumps at around a characteristic radius r_f (e.g., Shlosman & Begelman 1987, 1989; Goodman & Tan 2004; Levin 2007; Inayoshi & Haiman 2014; Latif & Schleicher 2015). The cooling time of the disk is estimated as

$$t_{\text{cool}} \approx \frac{\Sigma c_s^2/h}{\Lambda_{\text{H}^-}} = \frac{8}{9}(\alpha\Omega)^{-1}. \quad (9)$$

On the other hand, from Eqs. (2-5), the effective α parameter is given by

$$\alpha = \frac{G\dot{M}Q}{3c_s^3} \propto T^{-3/2}. \quad (10)$$

In the outer disk, the gas temperature gradually decreases toward the center, the value of α increases inward and finally exceeds a critical value (i.e. $t_{\text{cool}}\Omega \lesssim 1$), which has been numerically calculated to be $\alpha_f \lesssim 1$ (e.g., Gammie 2001; Rice et al. 2003; Krumholz et al. 2007; Clark et al. 2011; Zhu et al. 2012). For our fiducial parameter set ($\dot{M} = 0.095 M_\odot \text{ yr}^{-1}$, $Q = 1.0$, $\alpha_f = 1.0$, $M_\bullet = 1.0 \times 10^5 M_\odot$), the disk fragmentation occurs at

$$r_f \sim 3.3 \times 10^{-2} \text{ pc}, \quad (11)$$

where the orbital period is $t_{\text{orb},f} = 2\pi/\Omega_f \simeq 1.8 \times 10^3 \text{ yr}$. We find that the disk properties around the fragmentation radius are

$$\Sigma \sim 270 \text{ g cm}^{-2} \left(\frac{r}{r_f}\right)^{-3/2}, \quad (12)$$

$$n \sim 1.4 \times 10^{10} \text{ cm}^{-3} \left(\frac{r}{r_f}\right)^{-3}, \quad (13)$$

$$h/r \sim 0.045 \left(\frac{r}{r_f}\right)^{1/2}, \quad (14)$$

$$T \sim 3800 \text{ K} \left(\frac{r}{r_f}\right)^{-0.16}. \quad (15)$$

Typical mass of the clumps can be estimated as

$$M_{c,0} \approx (2\pi h_f)^2 \Sigma_f \sim 28 M_\odot, \quad (16)$$

where $2\pi h_f$ corresponds to the wavelength of the most unstable mode.

After fragmentation, the clumps grow in mass and migrate inward by interacting with the disk. The mass accretion rate onto the clump can be estimated as

$$\dot{M}_c = \frac{3}{2} \Sigma_f \Omega_f (f_H R_H)^2 \sim 1.6 \times 10^{-2} f_H^2 M_\odot \text{ yr}^{-1}, \quad (17)$$

where $R_H = r_f(M_{c,0}/3M_\bullet)^{1/3}$ is the Hill radius of the clump and $f_H \sim O(1)$. The initial migration time of the clump, during which the rotation radius typically decreases to $\sim r_f/2$, can be approximately given by Type I migration time (Zhu et al. 2012),

$$t_{\text{mig}} \approx \frac{1}{4Cq_f\mu_f} \left(\frac{h_f}{r_f}\right)^2 \frac{2\pi}{\Omega_f} \sim 1.3 \times 10^4 \text{ yr}, \quad (18)$$

where $C = 3.2 + 1.468 \xi$ with $\xi \approx 1.5$ being the power index of the surface density, $q_f = M_{c,0}/M_\bullet$, and $\mu_f = \pi \Sigma_f r_f^2/M_\bullet$ (Tanaka et al. 2002). From Eqs. (17-18), the total clump mass could increase to $M_c \sim 200 M_\odot$ during the migration time ($\sim 10 t_{\text{orb},f}$). This total mass is comparable to the isolation mass (e.g., Goodman & Tan 2004);

$$M_{\text{iso}} \approx \frac{(2\pi f_H \Sigma r^2)^{3/2}}{9M_\bullet^{1/2}} \sim 180 f_H^{3/2} \left(\frac{r}{r_f/2}\right)^{3/4} M_\odot, \quad (19)$$

and a gap can be formed around the clump. This also means that a reasonable fraction of the gas at the fragmentation radius can accrete onto at most a few clumps. Typical clump mass at $\sim r_f/2$ will range from $M_c = \text{a few} \times (10 - 100) M_\odot$, which is broadly consistent with numerical simulations of a self-gravitating disk around a SMS (Sakurai et al. 2015).

2.1.2. Star formation²

Just after the fragmentation, the central core of the clump collapses in a runaway fashion via optically-thin H^- free-bound emission. The core finally becomes optically thick and a quasi-hydrostatic equilibrium state, i.e., a protostar is formed, within a free-fall time of $\sim 500 \text{ yr} (n_f/10^{10} \text{ cm}^{-3})^{-1/2}$. During the migration time, the clumps grow via gas accretion at a rate of $\sim 2 \times 10^{-2} M_\odot \text{ yr}^{-1}$ (Eq. 17), which is higher than a critical value, $\dot{M}_{\text{crit}} \sim 4 \times 10^{-3} M_\odot \text{ yr}^{-1}$ (Omukai & Palla 2003). In this case, the protostellar structure consists of two parts; a bloated convective envelope with a radius of $R_c \sim 100 (2000) R_\odot$ for $M_c \sim 10 (100) M_\odot$ and a radiation dominated core which dominates the mass (Hosokawa et al. 2012, 2013).

The core contract within a Kelvin-Helmholtz (KH) time;

$$t_{\text{KH}} \approx 3600 \text{ yr } \beta_*^{-0.053} (1 - \beta_*)^{0.89}, \quad (20)$$

and evolves to a Pop III main-sequence star with a mass of

$$\frac{M_*}{M_\odot} \approx 52 \frac{\sqrt{1 - \beta_*}}{\beta_*^2}, \quad (21)$$

and a radius of

$$\frac{R_*}{R_\odot} \approx 4.5 \frac{(1 - \beta_*)^{0.39}}{\beta_*^{0.95}}, \quad (22)$$

where β_* is the dimensionless parameter roughly corresponding to the ratio of the gas pressure to the total pressure (Goodman & Tan 2004). For example, we can estimate $t_{\text{KH}} = 1.3 (0.74) \times 10^4 \text{ yr}$, $M_* = 40 (100) M_\odot$, and $R_* = 3.1 (5.3) R_\odot$. After a migration time (Eq. 18),

² Aykutaalp et al. (2014) discussed Pop III star formation in halos hosting a DCBH but at greater distances from the center.

the clump mass is close to the isolation mass of the disk and a gap will be formed. Then, gas accretion onto each clump will significantly decrease, which sets the maximum mass of the star to be a few $100 M_\odot$. We note that, although multiple stars can be formed from a single clump, the mean stellar mass is not much smaller than the total clump mass if the mass function is top-heavy, which is likely in the case of star formation from metal-poor gas (e.g. Hirano et al. 2014).

The main-sequence time of stars with $\langle M_* \rangle \sim 30 - 100 M_\odot$ is

$$t_{\text{MS}} \approx \frac{\epsilon_{\text{nuc}} M_* c^2}{L_*} \sim (2 - 4) \text{ Myr}, \quad (23)$$

where $\epsilon_{\text{nuc}} \sim 0.01$ is the energy conversion rate in nuclear burning and L_* is close to the Eddington luminosity (Schaerer 2002). Massive Pop III stars with a sufficient rotation would evolve into red supergiants after the main-sequence phase. This is primarily due to a rotational and convective mixing of CNO elements into the outer envelope (e.g., Hirschi 2007; Ekström et al. 2008). Finally, such massive Pop III stars collapse and supernova explosions occur, leading to metal enrichment in the nuclear region of the host halo, although the outcome will be sensitive to the stellar mass, rotation, and magnetic field (e.g., Joggerst et al. 2010; Joggerst & Whalen 2011; Yoon et al. 2012). Since we are interested in a few Myr after the DCBH formation, which is comparable to the main-sequence lifetime (Eq. 23), hereafter we only consider the main-sequence phase.

2.2. Inner slim disk

In the inner region, the disk finally becomes optically thick to H^- free-bound absorption when $\alpha_{\text{H}^-} r \gtrsim 1$, which is $r \lesssim 2.6 \times 10^{-4} \text{ pc}$ for our fiducial case. Here, $\alpha_{\text{H}^-} = 4\pi\Lambda_{\text{H}^-}/B(T)$ is the absorption coefficient and $B(T) = \sigma_{\text{SB}}T^4/\pi$. Note that we take r instead of h as the path length of the photon. The photons can escape mainly in the radial direction since optically thick ionized layers are formed above the thin disk due to the irradiation as we show in the next subsection.

Once the disk becomes optically thick to H^- free-bound absorption, both of the temperature and ionization fraction of the disk start to increase due to viscous heating. The accretion rate is super-Eddington with respect to Thomson scattering in fully ionized gas, $\dot{M} \gtrsim 500 L_{\text{Edd}}/\dot{c}^2$. Thus, once the disk is significantly ionized, the inner disk becomes the so-called slim disk (Abramowicz et al. 1988; Beloborodov 1998). The scale height of the slim disk takes its maximum at a radius where the radiation pressure dominates the gas pressure. In our case, this occurs at

$$r_{\text{edge}} \approx \left[\frac{3(1 - \eta_*)GM_*\dot{M}}{8\pi\sigma_{\text{SB}}T_{\text{edge}}^4} \right]^{1/3} \sim 10^{-4} \text{ pc}, \quad (24)$$

with $T_{\text{eff,edge}} \sim 10^4 \text{ K}$ being the effective temperature at the outer edge of the inner disk. In $r < r_{\text{edge}}$, the temperature scales as $T_{\text{eff}} \approx T_{\text{eff,edge}}(r/r_{\text{edge}})^{-1/2}$ and the aspect ratio of the disk becomes $h/r \gtrsim 0.3$. We note that ionization instability can occur in this transition region between the outer thin and inner slim disk, which

may result in an episodic accretion (e.g., Lin & Shields 1986).

Given that the accretion rate is well above the Eddington rate, a radiation-driven wind will be launched from the inner disk. Also, if large-scale magnetic fields exist in the innermost region, a relativistic jet can be launched by the Blandford-Znajek mechanism (Blandford & Znajek 1977). The total bolometric luminosity can be as large as $L_{\text{AGN}} \approx \eta_{\text{AGN}}(1 - \eta_*)\dot{M}c^2$, or

$$L_{\text{AGN}} \sim 7.4 \times 10^{44} \eta_{\text{AGN}}(1 - \eta_*) \text{ erg s}^{-1}. \quad (25)$$

The efficiency η_{AGN} is estimated to be $\sim 10\%$ for the disk wind (e.g., Ohsuga et al. 2005; Jiang et al. 2014; Sądowski et al. 2014) and can be even larger for the jet (Tchekhovskoy et al. 2011). Such disk wind and jet can give significant radiative and mechanical feedback on the parent halo, especially in the polar region. Although direct emission from the wind and jet are not detectable from $z \gtrsim 10$, the feedback effects can be indirectly probed by observing reprocessed emission, in particular $\text{H}\alpha$ and $\text{HeII } \lambda 1640$ with JWST (e.g., Johnson et al. 2011).

2.3. The effects of irradiation

Here, we consider the effect of irradiation of EUV photons from the inner region on the outer neutral disk. Inside a critical radius, $r < r_{\text{pe}} \approx GM_\bullet/c_{\text{s,HII}}^2 \sim 0.67 \text{ pc}$ ($M_\bullet/10^5 M_\odot$), optically-thick ionized layers with a scale height of $h_{\text{HII}} \approx c_{\text{s,HII}}/\Omega$ is formed above the outer disk. Here, $c_{\text{s,HII}} \sim 20 \text{ km s}^{-1}$ is the sound speed in the ionized region. Outside the critical radius, $r_{\text{pe}} < r < r_{\text{d}}$, the disk is photo-evaporated by the irradiation. The evaporation rate is estimated as $\dot{M}_{\text{pe}} \sim 6.6 \times 10^{-2} M_\odot \text{ yr}^{-1} (\Phi/10^{50} \text{ s}^{-1})^{1/2} (r_{\text{d}}/\text{pc})^{1/2}$, where Φ is the ionizing photon number, and gas supply from large scales onto the outer disk can be suppressed when $\dot{M}_{\text{pe}}/\dot{M} \gtrsim 0.2$ (Tanaka et al. 2013). The critical ionization photon number flux at the disk radius is $\Phi_{\text{crit}} \sim 9.5 \times 10^{50} \text{ s}^{-1} (r_{\text{d}}/\text{pc})^{-1} (\dot{M}/0.1 M_\odot \text{ yr}^{-1})^2$.

Before the direct collapse occurs, the main irradiation source is the central SMS. The accretion disk merges to the SMS at the surface, $R_{\text{sms}} \sim 3 \times 10^{-4} \text{ pc}$. The surface temperature of the SMS can be as high as $T_{\text{sms}} \sim 10^4 \text{ K}$ just before the direct collapse. The ionization photon flux can be $\Phi_{\text{sms}} \sim 10^{50} \text{ s}^{-1}$ (Hosokawa et al. 2013), which is still below the critical value.

Once the DCBH is formed, the accretion disk extends inward to the BH horizon scale. High-energy photons emitted from the inner slim disk are shielded by the slim disk itself. Instead, the outer disk is mainly irradiated by the outer edge of the slim disk, where $T_{\text{edge}} \sim 10^4 \text{ K}$ and $r_{\text{edge}} \sim 10^{-4} \text{ pc}$ (see Fig. 1 and §2.2). The corresponding ionization photon number flux is $\Phi_{\text{edge}} \sim 10^{49} \text{ s}^{-1}$, which is also below the critical value.

Finally, massive Pop III stars formed by disk fragmentation can be an important irradiation source. The ionization flux from each star is $\Phi_* \sim 2 \times 10^{49} \text{ s}^{-1} (M_*/40 M_\odot)^{3/2}$. About $\sim \text{Myr}$ after the DCBH formation, the total stellar mass becomes $\approx \eta_* M_\bullet$, where $\eta_* = 0.1$ is the star formation efficiency, and the number of stars can be $N_* \approx \eta_* M_\bullet / \langle M_* \rangle \sim 250$. Then, the total ionization flux can be $\Phi_{\text{cluster}} \approx N_* \Phi_* \sim 5 \times 10^{51} \text{ s}^{-1}$, which is larger than the critical value. Thus, we can con-

cluded that the radiative feedback from the nuclear star cluster can significantly suppress the disk accretion rate after a mass doubling time of the DCBH.

We note that massive stars also ionize the gas within the disk thickness, but the size of the ionized regions will be much smaller than the disk radius (Inayoshi & Haiman 2014). The outer thin disk is still predominantly neutral except near the disk surface even after the star formation. Thus our assumption in Sec. 2.1 is justified.

2.4. The effect of metal and dust

In Sec. 2.1, we assume that the disk consists of pristine gas, and consider only H^- emission as the radiative cooling process. Here, we discuss whether this assumption would be valid for a low-metallicity environment as well.

Even at $z \gtrsim 10$, the metallicity in an atomic-cooling halo could be as high as $Z \sim 10^{-3} - 10^{-4} Z_\odot$ due to past supernova explosions (e.g. Bromm et al. 2003; Whalen et al. 2008; Greif et al. 2010; Wise et al. 2012; Ritter et al. 2012), although the uncertainties are fairly large depending on the evolution history of each halo and on stellar progenitors which occur the explosions. We can neglect metal line cooling in the atomic-cooling halo as long as $Z \lesssim 10^{-3} Z_\odot$. On the other hand, thermal emission from dust grains could be an important coolant even if the metallicity is as low as $\sim 10^{-4} Z_\odot$ (Omukai et al. 2008).

In a low density region in the atomic cooling halo, the dust and gas are essentially decoupled. Due to the efficient emission, the dust temperature is kept much lower than surrounding gases, $T_d \sim 100$ K. When the gas density increases toward the center of the nuclear disk, the dust and gas start to exchange heat by collisions within the dynamical time, which occurs when

$$n \gtrsim 3 \times 10^9 \text{ cm}^{-3} \left(\frac{T}{4000 \text{ K}} \right) \left(\frac{f_{\text{dep}}}{0.1} \right)^{-2} \left(\frac{Z}{10^{-4} Z_\odot} \right)^{-2}, \quad (26)$$

(Schneider et al. 2006, 2012), where f_{dep} is the dust depletion factor. From Eqs. (8) and (15), the above condition is realized at $r \lesssim r_f$ for $Z \sim 10^{-4} Z_\odot$.

On the other hand, dust grains are sublimated once the dust temperature exceed a critical value of $\sim 10^3$ K. Considering the inner slim disk as the main irradiation source, the dust temperature is estimated as $T_d \approx T_{\text{edge}}(r/r_{\text{edge}})^{-1/2}$. Therefore, the effect of dust cooling could be neglected within ~ 0.01 pc, which is close to the typical star formation radius, $r \sim r_f/2$.

From the above arguments, we conclude that the dust cooling can be neglected if the gas metallicity in the atomic cooling halo is as low as $Z \lesssim 10^{-4} Z_\odot$. Otherwise, the dust cooling becomes important at $r > r_f$ and the nuclear accretion disk is more likely to fragment into clumps at larger radii than we showed in Sec. 2.1. The initial mass function of the stars formed by disk fragmentation would be less top-heavy compared with the metal-zero case (Omukai et al. 2008). Also, the size of the star cluster would be larger, resulting in a longer relaxation time. Thus, these effects could reduce the total event rate of energetic TDEs by DCBHs (see Sec. 3).

3. STELLAR TIDAL DISRUPTIONS BY

DIRECT COLLAPSE BLACK HOLES

3.1. Sending stars to the tidal radius

The orbits of the clumps and stars after the initial migration time is highly nonlinear and stochastic (e.g. Zhu et al. 2012). Three-dimension hydrodynamical simulations are required to predict the evolution. If the gas-to-star conversion efficiency is not extremely high, interactions between the stars and residual gas disk will be still effective. The stars may migrate further inward with a timescale of Eq. (18), or a viscous timescale once a gap is formed around the star (e.g., Lin & Papaloizou 1986; Ward 1997);

$$t_{\text{vis}} \approx \frac{1}{3\pi\alpha} \left(\frac{r}{h} \right)^2 \frac{2\pi}{\Omega} \sim 9.5 \times 10^4 \text{ yr}. \quad (27)$$

Such migration may proceed down at least to the radius where the disk mass becomes comparable to the clump mass, i.e., $\sim 10^{-4}$ pc for our fiducial case. Before the direct collapse, most of the clumps may merge with the central SMS with a stellar radius of $\sim 10^{-3}$ pc, as observed in numerical simulations (Sakurai et al. 2015). On the other hand, after the direct collapse, a dominant fraction of the stars will not directly migrate to the tidal radius of the DCBH, $r_t = R_*(M_\bullet/M_*)^{1/3} \sim 4.9 \times 10^{12} \text{ cm} (M_\bullet/10^5 M_\odot)^{1/3} (M_*/40 M_\odot)^{-1/3} (R_*/5 R_\odot)$. Instead, interactions between the clumps and stars finally become more relevant, resulting in forming a nuclear star cluster.

Motivated by the argument in Sec. 2.1.2, we assume the effective stellar mass $\langle M_* \rangle = 40 M_\odot$ and size of the cluster $\lesssim r_f/2 \sim 0.01$ pc, respectively. Initially, most of the stars are aligned with the disk. The relaxation time of the eccentricity can be estimated as (Stewart & Ida 2000; Kocsis & Tremaine 2011)

$$t_{\text{relax,disk}} \approx 0.22 \frac{\langle e^2 \rangle^2 M_\bullet^2}{\Omega \langle M_* \rangle \Sigma_* r^2 \ln \Lambda} \sim 3.7 \times 10^4 \text{ yr} \left(\frac{N_*}{10} \right)^{-1}. \quad (28)$$

Here, $\langle e^2 \rangle^{1/2} = 0.3$ is the mean eccentricity, $\Sigma_* = N_* \langle M_* \rangle / \pi r^2$ is the surface density of the stars, and $\Lambda = \langle e^2 \rangle^{3/2} M_\bullet / \langle M_* \rangle$. The inclination also relaxes with a timescale of $\approx 2 t_{\text{relax,disk}}$. A dozen of disk stars are formed within $\approx 10 \times \langle M_* \rangle / (\eta_* \dot{M}) \sim 4 \times 10^4$ yr. Hence the disk stars will evolve into a quasi-spherical stellar cluster within $\lesssim 10^5$ yr. The relaxation time of the spherical cluster can be estimated as

$$t_{\text{relax,cluster}} \approx 0.34 \frac{\sigma^3}{G^2 \rho_* \langle M_* \rangle \ln \Lambda} \sim 7.7 \times 10^4 \text{ yr}, \quad (29)$$

As for Eq. (29), we consider non-resonant two-body interaction (Binney & Tremaine 2008), substituting $\sigma = (GM_\bullet/2r)^{1/2}$, $\rho_* = \eta_* M_\bullet / (4\pi r^3/3)$, and $\ln \Lambda = \ln(M_\bullet / \langle M_* \rangle) \sim 7.8$. Some stars in the cluster are scattered onto the loss cone orbits within

$$t_{\text{tde}} \approx t_{\text{relax,cluster}} \times \ln(2/\theta_{\text{lc}}) \sim 3.8 \times 10^5 \text{ yr}, \quad (30)$$

where $\theta_{\text{lc}}^2 = (r_t/r) \times (GM_\bullet/\sigma^2)$ is the angular size of the loss cone (e.g., Syer & Ulmer 1999). From Eqs. (23) and (30), TDEs can occur within the lifetime of a massive Pop III star. Namely, we can expect $\approx t_{\text{MS}}/t_{\text{tde}} \sim 10$ of TDEs by each DCBH. We note that Eq. (29) is derived

assuming a continuous distribution function of stars. In our case, the number of stars $N_* \lesssim 1000$ may not be large enough, resulting in a relatively large scatter in the number of TDE per DCBH.

3.2. Observational signatures

Pop III stars disrupted by newborn DCBHs are massive and compact (see Eqs. 21-22). Consequently, the accretion luminosity of such TDEs can be significantly higher than the low- z events, and some associated emissions could be detectable even from high redshifts. The fallback accretion rate is estimated as

$$\dot{M}_{\text{fb}} \approx \frac{M_*}{3t_{\text{fb}}} \left(\frac{t}{t_{\text{fb}}} \right)^{-5/3}, \quad (31)$$

where

$$t_{\text{fb}} \sim 1.4 \times 10^5 \text{ s } k^{-3/2} \beta \times \left(\frac{M_\bullet}{10^5 M_\odot} \right)^{1/2} \left(\frac{M_*}{40 M_\odot} \right)^{-1} \left(\frac{R_*}{3 R_\odot} \right)^{3/2}, \quad (32)$$

is the fallback time, where k is a factor of $O(1)$ related to structure of disrupted star, β is the ratio between the tidal radius and pericenter distance (Stone et al. 2013). The peak accretion luminosity is $\dot{M}_{\text{fb}}/\dot{M} \sim 10^4$ times larger than the mean accretion rate.

If large-scale magnetic fields are amplified during the disruption, a relativistic jet can be launched by the Blandford-Znajek mechanism. The peak luminosity of the jet is estimated as $L_{\text{j,TDE}} \approx \eta_{\text{j}} M_* c^2 / 3t_{\text{fb}}$, or

$$L_{\text{j,TDE}} \sim 1.7 \times 10^{50} \text{ erg s}^{-1} \eta_{\text{j}} k^{3/2} \beta^{-1} \times \left(\frac{M_\bullet}{10^5 M_\odot} \right)^{-1/2} \left(\frac{M_*}{40 M_\odot} \right)^2 \left(\frac{R_*}{3 R_\odot} \right)^{-3/2} \quad (33)$$

With the super-Eddington accretion rate associated with TDEs, the innermost disk can be a magnetically arrested disk with an advection-dominated accretion flow (Tchekhovskoy et al. 2011). In this case, the jet efficiency can be described as

$$\eta_{\text{j}} \sim 1.3 \left(\frac{h/r}{0.3} \right) \left(\frac{a}{M_\bullet} \right)^2, \quad (34)$$

(Tchekhovskoy 2015). The Kerr parameter of DCBH is expected to be as large as $a/M_\bullet \sim 0.9$ (Reisswig et al. 2013). Thus, $\eta_{\text{j}} \sim 1$ is a viable assumption.

3.2.1. Prompt X rays

Although the prompt emission mechanism of TDE jets is still highly uncertain, the peak energy in the engine rest frame will be in hard-X-ray bands (Bloom et al. 2011; Levan et al. 2011; Burrows et al. 2011; Cenko et al. 2012), and observed in soft X-ray bands $\lesssim 10$ keV due to redshift. For an emission efficiency of 10% and a jet beaming factor of $f_{\text{b}} = 0.01$, the peak isotropic luminosity is $L_{\gamma, \text{iso}} \sim 8 \times 10^{50} \text{ erg s}^{-1}$, which corresponds to an observed flux of $\sim 6.3 \times 10^{-10} \text{ erg s}^{-1} \text{ cm}^{-2}$ from $z = 10$ and $\sim 1.3 \times 10^{-10} \text{ erg s}^{-1} \text{ cm}^{-2}$ from $z = 20$. The observed peak duration is $\delta t_{\text{obs}} \sim 10^{(5-6)} (1+z) \text{ s}$ for a disrupted star with $M_* = 40 M_\odot$. Such

emissions are good targets of soft-X-ray survey telescopes like eROSITA (Merloni et al. 2012) and HiZ-GUNDAM (Yonetoku et al. 2014). For example, eROSITA has a limiting flux of $\sim 10^{-12} \text{ erg s}^{-1} \text{ cm}^{-2}$, though the value depends on the emission spectrum (e.g., Khabibullin et al. 2014), and can detect the above emission even from $z \sim 20$. The early tail emission $\propto t_{\text{obs}}^{-5/3}$ is also detectable and can be used to distinguish this type of TDEs from other high- z transients (e.g., Kashiya et al. 2013; Matsumoto et al. 2015a). If the intrinsic spectrum is hard enough, the signal can be also detectable up to $z \sim 20$ by *Swift* BAT, but only with an integration time of $\gtrsim 10^4 \text{ s}$ (Baumgartner et al. 2013). A BAT archival data search of dim (in terms of the observed flux) and ultra-long transients will be interesting.

3.2.2. Radio afterglow

A promising counterpart may be the afterglow emission (e.g., Ioka & Mészáros 2005; Toma et al. 2011). The kinetic energy of the jet is as large as $E_{\text{j}} \approx L_{\text{j,TDE}} t_{\text{fb}} \sim 2.4 \times 10^{55} \text{ erg } (M_*/40 M_\odot)$. The jet kinetic energy is comparable or larger than the binding energy of the parent halo. Thus, TDEs in collapsing atomic-hydrogen-cooling halos will also give significant mechanical feedback. The synchrotron emission from the decelerating jet, especially in radio bands, could be detectable even from $z \sim 20$ by e.g., eVLA as we show below. In this subsection, we use the notation $Q = 10^x Q_x$ in CGS unit unless we note.

The typical time scale of the afterglow emission corresponds to the deceleration time of the TDE jet, $t_{\text{dec}} \approx (1+z)r_{\text{dec}}/4\Gamma^2 c$, or

$$t_{\text{dec}} \sim 1.0 \times 10^7 \text{ s } \left(\frac{1+z}{11} \right) f_{\text{b},-2}^{-1} E_{\text{j},55} \Gamma_{1.3}^{-4} \dot{M}_{\text{w},-2}^{-1} v_{\text{w},10}. \quad (35)$$

in the observer frame. Here, Γ is the Lorentz factor of the jet and $r_{\text{dec}} \approx E_{\text{j}} v_{\text{w}} / f_{\text{b}} \dot{M}_{\text{w}} \Gamma^2 c^2$, or

$$r_{\text{dec}} \sim 4.4 \times 10^{19} \text{ cm } f_{\text{b},-2}^{-1} E_{\text{j},55} \Gamma_{1.3}^{-2} \dot{M}_{\text{w},-2}^{-1} v_{\text{w},10}, \quad (36)$$

is the deceleration radius. We assume a wind-like density profile; $\rho_{\text{w}}(r) = \dot{M}_{\text{w}}/4\pi v_{\text{w}} r^2$, and assume that $\dot{M}_{\text{w}} = 10^{-2} M_\odot \text{ yr}^{-1}$ and $v_{\text{w}} = 10^{10} \text{ cm s}^{-1}$ as fiducial, which corresponds to that a 10 % of the accreted matter has been ejected from the slim disk with an escape velocity at the inner most region. Note that the first TDE typically occurs $t_{\text{tde}} \gtrsim 10^5 \text{ yr}$ after the DCBH formation when the wind region extends far beyond the deceleration radius, $r_{\text{dec}} \ll v_{\text{w}} t_{\text{tde}}$.

At the decelerating shock, magnetic field amplification and electron acceleration can occur. The comoving magnetic field strength at the forward shock is estimated as $B \approx [32\pi\epsilon_B \rho_{\text{w}}(r_{\text{dec}}) c^2 \Gamma^2]^{1/2}$, or

$$B \sim 0.031 \text{ G } \epsilon_B^{1/2} f_{\text{b},-2} \dot{M}_{\text{j},55}^{-1} \Gamma_{1.3}^3 \dot{M}_{\text{w},-2}^{3/2} v_{\text{w},10}^{-3/2}, \quad (37)$$

where ϵ_B is the magnetic field amplification efficiency. We note that the energy density of the cosmic microwave background (CMB) in the comoving frame is much smaller than that of the amplified magnetic field, thus the effect of inverse Compton cooling can be neglected, unlike extended lobes produced by steady jets

from high- z SMBHs whose radio emission may be muted by the CMB (Celotti & Fabian 2004; Ghisellini et al. 2014; Fabian et al. 2014). The minimum Lorentz factor of the non-thermal electrons is given by

$$\gamma_{e,m} \approx \epsilon_e \frac{p-2}{p-1} \frac{m_p}{m_e} \Gamma \sim 1200 \epsilon_{e,-1} \Gamma_{1.3}. \quad (38)$$

where ϵ_e is the acceleration efficiency. Hereafter we set the power law index of the non-thermal electrons as $p = 2.5$. The characteristic synchrotron frequency in the observer frame is $\nu_m = \Gamma \gamma_{e,m}^2 qB / [2\pi m_e c(1+z)]$, or

$$\nu_m \sim 230 \text{ GHz} \left(\frac{1+z}{11} \right)^{-1} \epsilon_{e,-1}^2 \epsilon_{B,-2}^{1/2} \times f_{b,-2} E_{j,55}^{-1} \Gamma_{1.3}^6 \dot{M}_{w,-2}^{3/2} v_{w,10}^{-3/2}, \quad (39)$$

and the corresponding flux can be estimated as

$$F_{\nu,\max} \approx \frac{\sigma_T m_e c^2 \dot{M}_w B \Gamma r_{\text{dec}} (1+z)}{12\pi q m_p v_w D_L^2} \sim 360 \text{ mJy} \left(\frac{1+z}{11} \right) D_{L,29.5}^{1/2} \epsilon_{B,-2}^{1/2} \Gamma_{1.3}^2 \dot{M}_{w,-2}^{3/2} v_{w,10}^{-3/2}, \quad (40)$$

where D_L is the luminosity distance to the source. For $\nu \lesssim \nu_m$, the flux proportional to $\nu^{1/3}$ (e.g., Granot & Sari 2002). Note that in our fiducial case, the shocked plasma is in the slow cooling regime and synchrotron self absorption is not relevant for $\nu \gtrsim \text{GHz}$ at $t \sim t_{\text{dec}}$. For example, at $\nu \sim 1-10 \text{ GHz}$, the anticipated peak flux $\sim 10^6 (1+z)$ s after the TDE can be $\gtrsim 10 \text{ mJy}$ even from $z \sim 20$, which can be detectable by eVLA and SKA.

3.2.3. Disk emission

Finally, the quasi-thermal disk emission can be also enhanced by the TDEs. In our case, the emission temperature is in EUV or soft-X-ray bands and the luminosity may be still close to the Eddington value, $\sim 10^{43} \text{ erg s}^{-1}$ (Piran et al. 2015). Given the intergalactic absorption, such emissions from high- z events are difficult to be detected by on-going and up-coming transient surveys.

3.3. Event rate

We briefly estimate the rate of such high- z TDEs. The comoving number density of SMSs or DCBHs in the early growth is estimated to be $\sim 10^{-3} \text{ Mpc}^{-3} z^{-1}$ for $z \gtrsim 10$ (Johnson et al. 2013), which corresponds

to $\sim 100 \text{ deg}^{-2}$ of such systems in the sky. Given ~ 10 TDEs by each DCBH and a jet beaming factor of $f_b \sim 0.01$, the total rate at $z \sim 10-20$ is estimated to be a few $\text{sky}^{-1} \text{yr}^{-1}$.

Note that uncertainties of the DCBH number density are fairly large at this stage and can be significantly larger than the above value (see e.g., Agarwal et al. 2012; Yue et al. 2014). Also, if the inward migration of the stars before joining the cluster is more efficient, the size of the star cluster becomes significantly smaller than the disk fragmentation radius, in which case the TDE rate is enhanced. On the other hand, relativistic jets may not accompany in some cases e.g., due to absence of large-scale magnetic field amplification in the TDE disk. In fact, off-axis radio afterglow observations of local TDEs suggest that only $\lesssim 10\%$ of them are accompanied by powerful relativistic jets (van Velzen et al. 2013; Bower et al. 2013).

4. SUMMARY

We analytically calculate properties of a nuclear accretion disk around a direct collapse black hole (DCBH) within a few Myr after its formation. The outer disk is gravitationally unstable and fragments into clumps at $\sim 0.01-0.1 \text{ pc}$. The clumps evolve into Pop III stars with a typical mass of $\sim 10-100 M_\odot$, which will form a dense star cluster. The relaxation time of the cluster is estimated to be $\sim 10^5 \text{ yr}$ and shorter than the stellar lifetime of a few Myr. We can expect that ~ 10 of massive metal-poor stars are tidally disrupted by each DCBH. If a relativistic jet is launched by such a tidal disruption event, bright X-ray transients with a duration of a few months to $\sim \text{yr}$ could be produced and detectable by *Swift* BAT and eROSITA even from $z \sim 20$. Given a formation rate of DCBHs $\sim 10^{-3} \text{ Mpc}^{-3} z^{-1}$, the all sky event rate could be a few times per year, although the uncertainties are fairly large. Around the time when the DCBH mass is doubled, gas accretion will be strongly suppressed by various AGN feedback effects; the radiative and mechanical feedback from the inner slim disk, star cluster, and TDE jets, which can be probed by follow-up observations by eVLA and JWST.

ACKNOWLEDGEMENTS

We thank Zoltán Haiman, Nicholas Stone, Kunihiro Ioka, and Amy Lien for valuable comments. KK is supported by NASA through Einstein Postdoctoral Fellowship grant number PF4-150123 awarded by the Chandra X-ray Center, which is operated by the Smithsonian Astrophysical Observatory for NASA under contract NAS8-03060. KI is supported by the Simons Foundation through the Simons Society of Fellows.

REFERENCES

- Abramowicz, M. A., Czerny, B., Lasota, J. P., & Szuszkiewicz, E. 1988, *ApJ*, 332, 646
- Agarwal, B., Khochfar, S., Johnson, J. L., et al. 2012, *MNRAS*, 425, 2854
- Agarwal, B., Smith, B., Glover, S., Natarajan, P., & Khochfar, S. 2015, *arXiv:1504.04042*
- Aykutalp, A., Wise, J. H., Spaans, M., & Meijerink, R. 2014, *ApJ*, 797, 139
- Baumgarte, T. W., & Shapiro, S. L. 1999, *ApJ*, 526, 941
- Baumgartner, W. H., Tueller, J., Markwardt, C. B., et al. 2013, *ApJS*, 207, 19
- Becerra, F., Greif, T. H., Springel, V., & Hernquist, L. E. 2015, *MNRAS*, 446, 2380
- Begelman, M. C., Volonteri, M., & Rees, M. J. 2006, *MNRAS*, 370, 289
- Beloborodov, A. M. 1998, *MNRAS*, 297, 739
- Binney, J., & Tremaine, S. 2008, *Galactic Dynamics: Second Edition* (Princeton University Press)
- Blandford, R. D., & Znajek, R. L. 1977, *MNRAS*, 179, 433

- Bloom, J. S., Giannios, D., Metzger, B. D., et al. 2011, *Science*, 333, 203
- Bower, G. C., Metzger, B. D., Cenko, S. B., Silverman, J. M., & Bloom, J. S. 2013, *ApJ*, 763, 84
- Bromm, V., & Loeb, A. 2003, *ApJ*, 596, 34
- Bromm, V., Yoshida, N., & Hernquist, L. 2003, *ApJ*, 596, L135
- Burrows, D. N., Kennea, J. A., Ghisellini, G., et al. 2011, *Nature*, 476, 421
- Celotti, A., & Fabian, A. C. 2004, *MNRAS*, 353, 523
- Cenko, S. B., Krimm, H. A., Horesh, A., et al. 2012, *ApJ*, 753, 77
- Chandrasekhar, S. 1964, *ApJ*, 140, 417
- Clark, P. C., Glover, S. C. O., Smith, R. J., et al. 2011, *Science*, 331, 1040
- Ekström, S., Meynet, G., Chiappini, C., Hirschi, R., & Maeder, A. 2008, *A&A*, 489, 685
- Fabian, A. C., Walker, S. A., Celotti, A., et al. 2014, *MNRAS*, 442, L81
- Gammie, C. F. 2001, *ApJ*, 553, 174
- Gardner, J. P., Mather, J. C., Clampin, M., et al. 2006, *Space Sci. Rev.*, 123, 485
- Gehrels, N., Chincarini, G., Giommi, P., et al. 2004, *ApJ*, 611, 1005
- Ghisellini, G., Celotti, A., Tavecchio, F., Haardt, F., & Sbarbato, T. 2014, *MNRAS*, 438, 2694
- Goodman, J., & Tan, J. C. 2004, *ApJ*, 608, 108
- Granot, J., & Sari, R. 2002, *ApJ*, 568, 820
- Greif, T. H., Glover, S. C. O., Bromm, V., & Klessen, R. S. 2010, *ApJ*, 716, 510
- Haiman, Z. 2013, in *Astrophysics and Space Science Library*, Vol. 396, *Astrophysics and Space Science Library*, ed. T. Wiklund, B. Mobasher, & V. Bromm, 293
- Hartwig, T., Latif, M. A., Magg, M., et al. 2015, *ArXiv e-prints*
- Hirano, S., Hosokawa, T., Yoshida, N., et al. 2014, *ApJ*, 781, 60
- Hirschi, R. 2007, *A&A*, 461, 571
- Hosokawa, T., Omukai, K., & Yorke, H. W. 2012, *ApJ*, 756, 93
- Hosokawa, T., Yorke, H. W., Inayoshi, K., Omukai, K., & Yoshida, N. 2013, *ApJ*, 778, 178
- Iben, Jr., I. 1963, *ApJ*, 138, 1090
- Inayoshi, K., & Haiman, Z. 2014, *MNRAS*, 445, 1549
- Inayoshi, K., Hosokawa, T., & Omukai, K. 2013, *MNRAS*, 431, 3036
- Inayoshi, K., & Omukai, K. 2012, *MNRAS*, 422, 2539
- Inayoshi, K., Omukai, K., & Tasker, E. 2014, *MNRAS*, 445, L109
- Inayoshi, K., Visbal, E., & Kashiyaama, K. 2015, *MNRAS*, 453, 1692
- Ioka, K., & Mészáros, P. 2005, *ApJ*, 619, 684
- Jiang, Y.-F., Stone, J. M., & Davis, S. W. 2014, *ApJ*, 796, 106
- Joggerst, C. C., Almgren, A., Bell, J., et al. 2010, *ApJ*, 709, 11
- Joggerst, C. C., & Whalen, D. J. 2011, *ApJ*, 728, 129
- Johnson, J. L., Dalla Vecchia, C., & Khochfar, S. 2013, *MNRAS*, 428, 1857
- Johnson, J. L., Khochfar, S., Greif, T. H., & Durier, F. 2011, *MNRAS*, 410, 919
- Kashiyaama, K., Nakauchi, D., Suwa, Y., Yajima, H., & Nakamura, T. 2013, *ApJ*, 770, 8
- Khabibullin, I., Sazonov, S., & Sunyaev, R. 2014, *MNRAS*, 437, 327
- Kocsis, B., & Tremaine, S. 2011, *MNRAS*, 412, 187
- Krumholz, M. R., Klein, R. I., & McKee, C. F. 2007, *ApJ*, 656, 959
- Latif, M. A., & Schleicher, D. R. G. 2015, *MNRAS*, 449, 77
- Latif, M. A., Schleicher, D. R. G., & Hartwig, T. 2016, *MNRAS*, 458, 233
- Levan, A. J., Tanvir, N. R., Cenko, S. B., et al. 2011, *Science*, 333, 199
- Levin, Y. 2007, *MNRAS*, 374, 515
- Lin, D. N. C., & Papaloizou, J. 1986, *ApJ*, 309, 846
- Lin, D. N. C., & Shields, G. A. 1986, *ApJ*, 305, 28
- Lodato, G., & Natarajan, P. 2006, *MNRAS*, 371, 1813
- Matsumoto, T., Nakauchi, D., Ioka, K., Heger, A., & Nakamura, T. 2015a, *ApJ*, 810, 64
- Matsumoto, T., Nakauchi, D., Ioka, K., & Nakamura, T. 2015b, *arXiv:1512.03058*
- Merloni, A., Predehl, P., Becker, W., et al. 2012, *arXiv:1209.3114*
- Mortlock, D. J., Warren, S. J., Venemans, B. P., et al. 2011, *Nature*, 474, 616
- Ohsuga, K., Mori, M., Nakamoto, T., & Mineshige, S. 2005, *ApJ*, 628, 368
- Omukai, K. 2001, *ApJ*, 546, 635
- Omukai, K., & Palla, F. 2003, *ApJ*, 589, 677
- Omukai, K., Schneider, R., & Haiman, Z. 2008, *ApJ*, 686, 801
- Piran, T., Sądowski, A., & Tchekhovskoy, A. 2015, *MNRAS*, 453, 157
- Regan, J. A., & Haehnelt, M. G. 2009a, *MNRAS*, 396, 343
- . 2009b, *MNRAS*, 393, 858
- Regan, J. A., Johansson, P. H., & Haehnelt, M. G. 2014, *MNRAS*, 439, 1160
- Reisswig, C., Ott, C. D., Abdikamalov, E., et al. 2013, *Physical Review Letters*, 111, 151101
- Rice, W. K. M., Armitage, P. J., Bate, M. R., & Bonnell, I. A. 2003, *MNRAS*, 339, 1025
- Ritter, J. S., Safranek-Shrader, C., Gnat, O., Milosavljević, M., & Bromm, V. 2012, *ApJ*, 761, 56
- Sakurai, Y., Hosokawa, T., Yoshida, N., & Yorke, H. W. 2015, *MNRAS*, 452, 755
- Sądowski, A., Narayan, R., McKinney, J. C., & Tchekhovskoy, A. 2014, *MNRAS*, 439, 503
- Schaerer, D. 2002, *A&A*, 382, 28
- Schleicher, D. R. G., Palla, F., Ferrara, A., Galli, D., & Latif, M. 2013, *A&A*, 558, A59
- Schneider, R., Omukai, K., Bianchi, S., & Valiante, R. 2012, *MNRAS*, 419, 1566
- Schneider, R., Omukai, K., Inoue, A. K., & Ferrara, A. 2006, *MNRAS*, 369, 1437
- Shakura, N. I., & Sunyaev, R. A. 1973, *A&A*, 24, 337
- Shang, C., Bryan, G. L., & Haiman, Z. 2010, *MNRAS*, 402, 1249
- Shibata, M., & Shapiro, S. L. 2002, *ApJ*, 572, L39
- Shlosman, I., & Begelman, M. C. 1987, *Nature*, 329, 810
- . 1989, *ApJ*, 341, 685
- Stewart, G. R., & Ida, S. 2000, *Icarus*, 143, 28
- Stone, N., Sari, R., & Loeb, A. 2013, *MNRAS*, 435, 1809
- Sugimura, K., Omukai, K., & Inoue, A. K. 2014, *MNRAS*, 445, 544
- Syer, D., & Ulmer, A. 1999, *MNRAS*, 306, 35
- Tanaka, H., Takeuchi, T., & Ward, W. R. 2002, *ApJ*, 565, 1257
- Tanaka, K. E. I., Nakamoto, T., & Omukai, K. 2013, *ApJ*, 773, 155
- Tchekhovskoy, A. 2015, in *Astrophysics and Space Science Library*, Vol. 414, *Astrophysics and Space Science Library*, ed. I. Contopoulos, D. Gabuzda, & N. Kylafis, 45
- Tchekhovskoy, A., Narayan, R., & McKinney, J. C. 2011, *MNRAS*, 418, L79
- Toma, K., Sakamoto, T., & Mészáros, P. 2011, *ApJ*, 731, 127
- van Velzen, S., Frail, D. A., Körding, E., & Falcke, H. 2013, *A&A*, 552, A5
- Visbal, E., Haiman, Z., & Bryan, G. L. 2014, *MNRAS*, 445, 1056
- Volonteri, M. 2012, *Science*, 337, 544
- Ward, W. R. 1997, *Icarus*, 126, 261
- Whalen, D., van Veelen, B., O'Shea, B. W., & Norman, M. L. 2008, *ApJ*, 682, 49
- Wise, J. H., Turk, M. J., & Abel, T. 2008, *ApJ*, 682, 745
- Wise, J. H., Turk, M. J., Norman, M. L., & Abel, T. 2012, *ApJ*, 745, 50
- Wu, X.-B., Wang, F., Fan, X., et al. 2015, *Nature*, 518, 512
- Yonetoku, D., Mihara, T., Sawano, T., et al. 2014, in *Society of Photo-Optical Instrumentation Engineers (SPIE) Conference Series*, Vol. 9144, *Society of Photo-Optical Instrumentation Engineers (SPIE) Conference Series*, 2
- Yoon, S.-C., Dierks, A., & Langer, N. 2012, *A&A*, 542, A113
- Yue, B., Ferrara, A., Salvaterra, R., Xu, Y., & Chen, X. 2014, *MNRAS*, 440, 1263
- Zhu, Z., Hartmann, L., Nelson, R. P., & Gammie, C. F. 2012, *ApJ*, 746, 110